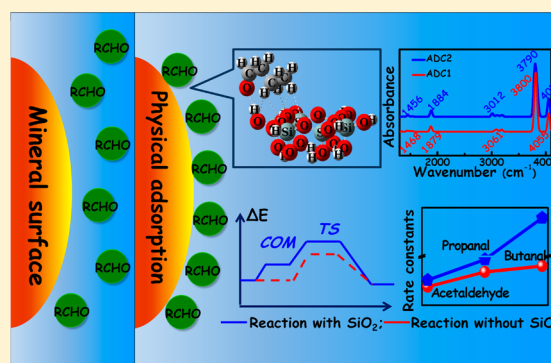


# Can Silica Particles Reduce Air Pollution by Facilitating the Reactions of Aliphatic Aldehyde and NO<sub>2</sub>?

Yuemeng Ji,<sup>†</sup> Honghong Wang,<sup>†,‡</sup> Jiangyao Chen,<sup>†</sup> Guiying Li,<sup>†</sup> Taicheng An,<sup>\*,†</sup> and Xiaolei Zhao<sup>§</sup><sup>†</sup>State Key Laboratory of Organic Geochemistry and Guangdong Key Laboratory of Environmental Resources Utilization and Protection, Guangzhou Institute of Geochemistry, Chinese Academy of Sciences, Guangzhou 510640, China<sup>‡</sup>University of Chinese Academy of Sciences, Beijing 100049, China<sup>§</sup>School of Physics and Chemistry, Henan Polytechnic University, Jiaozuo 454000, PR China

## S Supporting Information

**ABSTRACT:** This study investigated the heterogeneous atmospheric reactions of acetaldehyde, propanal, and butanal with NO<sub>2</sub> onto silica (SiO<sub>2</sub>) clusters using a theoretical approach. By analyzing spectral features and adsorption parameters, the formation of hydrogen bonds and negative adsorption energies provide evidence that an efficient spontaneous uptake of aliphatic aldehydes onto SiO<sub>2</sub> could occur. The atmospheric reaction mechanisms show that when aldehydes and NO<sub>2</sub> react on the surface model, the H atom abstraction reaction from the aldehydic molecule by NO<sub>2</sub> is an exclusive channel, forming nitrous acid and acyl radicals. This study included kinetics exploring the reaction of aldehydes with NO<sub>2</sub> using a canonical variational transition state theory. The reaction rate constants are increased in the presence of SiO<sub>2</sub> between the temperatures 217 and 298 K. This may explain how aldehydes can temporarily stay on mineral particles without chemical reactions. The results suggest that silica can depress the rate at which the studied aldehydes react with NO<sub>2</sub> and possibly reduce air pollution generated by these atmospheric reactions.



## INTRODUCTION

Mineral particles are a major natural component of atmospheric aerosols, making up nearly one-third to one-half of total annual aerosol emissions by mass.<sup>1</sup> Further, the potential reactive surface of mineral aerosols may serve as a significant sink for some atmospheric gases,<sup>1–4</sup> influencing the global photochemical oxidant budget.<sup>5,6</sup> All these highlight the importance of studying the effect and role mineral particles in altering atmospheric reactions.

Recent laboratory studies, field observations, and modeling calculations have demonstrated the importance of heterogeneous processes in volatile organic compounds (VOCs) reactions. For example, Zhao et al.<sup>7</sup> proposed that heterogeneous reactions onto  $\alpha$ -Al<sub>2</sub>O<sub>3</sub> are important sinks for methacrolein and methyl vinyl ketone (MVK) and may contribute to atmospheric organic aerosols. Using a diffuse reflectance infrared Fourier transform spectroscopy reactor, Tong et al.<sup>8</sup> found that the adsorption of atmospheric monocarboxylic acids onto mineral dust may compete with homogeneous loss pathways. Iuga et al., in turn, concluded that silicates are good sinks for trapping aldehydes and lowering the reaction rate of aldehydes with OH radicals.<sup>9</sup> However, the mechanisms and kinetics of atmospheric mineral particles in these heterogeneous chemical reactions are not fully understood.

In some places in developing countries, aldehydes and NO<sub>2</sub> are abundant in indoor and outdoor environments;<sup>10,11</sup> one example is the Pearl River Delta in South China. In these areas, abundant aldehydes and NO<sub>2</sub> in the air lead to a complex series of chemical transformations, resulting in photooxidant formation,<sup>12</sup> acid deposition and secondary particulate matter,<sup>13</sup> and photochemical smog.<sup>14</sup> Furthermore, the most important mineral particles of the clay fraction (<1  $\mu$ m) that can enter the troposphere from dust storms are phyllosilicates, such as Illite, kaolinite, chlorite, and smectite;<sup>15</sup> and coarser particles (>2  $\mu$ m) in dust storms mainly consist of quartz, feldspars, and carbonates.<sup>16</sup> Whether they are clay fraction or coarser particles, the large abundance of SiO<sub>2</sub> can be found in these mineral particles. As a result, silica and silicate mineral are richly present in atmospheric aerosols and are expected to play an important role in the heterogeneous chemistry of the troposphere.

Given this significance, this study researches the heterogeneous reaction of aldehydes with NO<sub>2</sub> onto SiO<sub>2</sub> cluster surfaces, using a theoretical approach. Study objectives were as follows: (i) determine the adsorption patterns of aliphatic aldehydes and NO<sub>2</sub> onto SiO<sub>2</sub> clusters; (ii) explore the detailed reaction mechanisms and kinetics of aliphatic aldehydes with

Received: September 17, 2015

Revised: October 18, 2015

Published: October 27, 2015

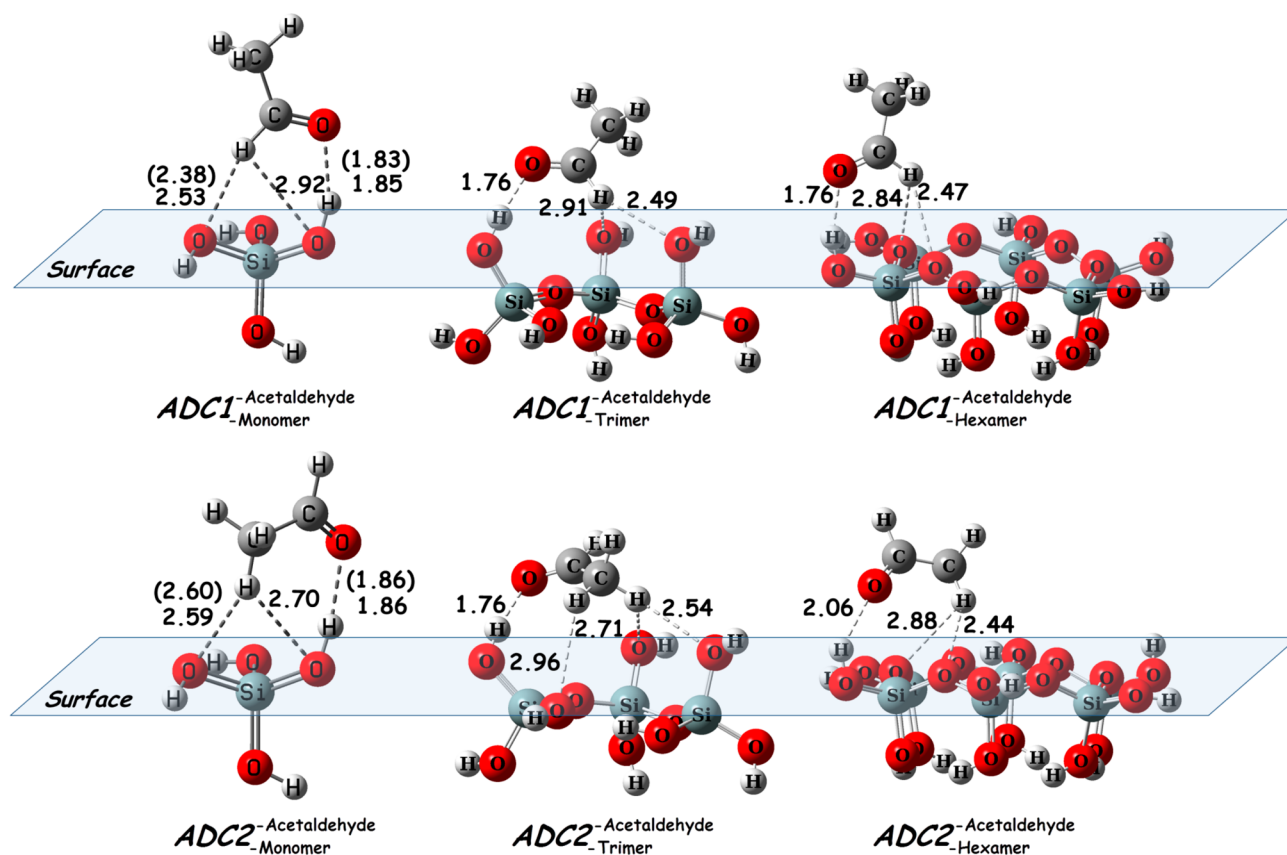


**Figure 1.** Geometries of adsorption complexes for acetaldehyde onto three surface models (in Å) as well as the available published data.<sup>9</sup> Here, acetaldehyde was allowed to move freely until it reached the optimum adsorption at the MPWB1K/6-311G(d,p) level.

NO<sub>2</sub> in the presence of mineral particles; (iii) establish a relationship between temperature and atmospheric height on the rate constants; and (iv) explore the effect of mineral particles on chemical reactions, and compare these data with available experimental data to test the theoretical model. This is a unique way to research these atmospheric heterogeneous reactions.

## METHODS

Quantum chemical calculations in this study were performed using the Gaussian 03 software package.<sup>17</sup> The hybrid density functional theory of the MPWB1K function, successfully used for calculations previously by our group<sup>18</sup> and others,<sup>19</sup> was also used for calculations. Additionally, a multicoefficient correlation method, named the BMC-CCSD method, was used to test model accuracy of the MPWB1K model. The BMC-CCSD is based on coupled cluster theory, with single and double excitations.<sup>20</sup>

At the MPWB1K/6-311G(d,p) level, the geometries were fully optimized, and the frequency calculations were conducted on all stationary points. This confirmed that all calculated lowest energy structures resided at the local minima on their respective potential energy surfaces (PES). At the same level, the transition states were verified to properly connect the reactants with the products by intrinsic reaction coordinate (IRC) theory. The MPWB1K function with the flexible 6-311++G(3df,3pd) basis set was applied to obtain a more reliable PES profile. A zero-point energy (ZPE) correction was implemented for the potential energy.

The adsorption energies were calculated using to eq 1:

$$\Delta E_{\text{ae}} = E_{\text{adsorption complex}} - (E_{\text{isolated molecule}} + E_{\text{surface model}}) \quad (1)$$

where  $E_{\text{adsorption complex}}$  is the total energy of the adsorption complex (ADS) and  $E_{\text{isolated molecule}} + E_{\text{surface model}}$  is the sum of the isolated reactant and the corresponding surface model. Both the counterpoise corrections for the basis set superposition error (BSSE correction) and zero-point energy (ZPE) corrections were not applied in this part, because the hybrid density functional theory without the counterpoise corrections has been shown to agree well with experimental results.<sup>21</sup>

The dual-level potential profile was adopted to study kinetics nature. In this approach, a few extra single-point (selected stationary points along the path) calculations were used to correct the lower-level result, using the interpolated single-point energy (ISPE) method.<sup>22</sup> In this paper, the dual-level dynamics approach is denoted as X//Y, where a single-point energy calculation at level X is carried out for the geometry optimized at a lower level Y. Both the rate constants and the product distributions of all the possible reaction pathways are calculated using the canonical variational transition state theory (CVT) method,<sup>23</sup> with a small curvature tunneling correction (SCT).<sup>24</sup> A more detailed description is included in the Supporting Information.

## RESULTS AND DISCUSSION

**Adsorption Mechanisms.** Most silica powders and gels are formed from extremely small particles of amorphous silica, or by porous aggregates with SiOH groups at the surface. Many siloxane Si-O-Si bridges and SiOH are also found on the external and internal surfaces of the natural clay mineral. Thus,

silicic acid is good for modeling  $\text{SiO}_2$  mineral particles, because the ideal surface of phyllosilicate has a large number of siloxane  $\text{Si-O-Si}$ .<sup>9,18,25,26</sup> For silicic acid surfaces, the structures should terminate either in a siloxane group with oxygen on the surface or in isolated, vicinal, and geminal silanols (Scheme S1). As Scheme S1 shows, an isolated silanol group is formed by one OH group bound to a Si atom. A geminal site should be two OH groups per Si atom, and a siloxane bridge group's structure consists of more than one  $\text{Si-O-Si}$  bridge.

Given this background, three different types of active sites require modeling with a properly chosen cluster: the isolated silanol, the geminal silanol, and the siloxane bridge groups. Although the natural clay surface presents many structural defects and fractures, its main acid sites are Brønsted sites. These sites are associated with aluminol and silanol groups; as such, the small clusters must accommodate isolated irregularly distributed sites in the quantum calculation.<sup>25–27</sup>

To more closely clarify the model, three silica-based clusters of  $\text{Si}_x\text{O}_y(\text{OH})_z$ , the monomer  $\text{Si}(\text{OH})_4$ , the trimer  $\text{Si}_3\text{O}_2(\text{OH})_8$ , and the hexamer  $\text{Si}_6\text{O}_6(\text{OH})_{12}$ , were chosen to simulate the silica surfaces of the isolated and geminal silanol groups and the siloxane bridge groups. This section of the paper discusses the adsorption mechanisms of aldehydes and  $\text{NO}_2$  onto these three surface models.

First, both the aldehydes and  $\text{NO}_2$  have opportunities to be adsorbed onto the  $\text{SiO}_2$  surface from the atmosphere. The adsorption structures, Cartesian coordinates, and energies listed in Figures 1, S1, and Table S1 show that the three studied aldehydes (acetaldehyde, propanal, and butanal) are more easily adsorbed onto the surface model. For example, the adsorption energy of  $\text{NO}_2$  onto the surface model,  $-2.48 \text{ kcal mol}^{-1}$ , is 2 times larger than those of three aldehydes. This indicates that the three aldehydes are more spontaneously adsorbed onto the surface model than  $\text{NO}_2$ . Therefore, in this work, we focused on investigating the adsorption mechanisms of the studied aldehydes onto surface models.

The geometries of acetaldehyde, propanal, and butanal adsorbed onto the monomer, trimer and hexamer surface models were optimized at the MPWB1K/6-311G(d,p) level (Figures 1, S2, and S3). When acetaldehyde, propanal, and butanal adsorbed onto the surface models, two kinds of adsorption patterns were seen. First, the aldehydic H atom ( $\text{H}_{\text{Ald}}$ ) interacted with an oxygen atom on the surface ( $\text{O}_{\text{SiO}_2}$ ), with the aliphatic chain extending away from the surface (denoted as ADC1). Second, the aldehydes interacted with the surface model mainly through the chain H atoms (denoted as ADC2), and the adsorption structures depend on the surface characteristics. To test the calculation reliability of the MPWB1K method on the adsorption model, Figures 1, S2, and S3 provide a comparison with other available data<sup>9</sup> related to the geometric parameters. The maximum error between the calculated and the experimental data was less than 5%, indicating the high reliability of the calculation methods used in this study.

The infrared spectra of acetaldehyde, propanal, and butanal adsorbed onto the surface models were also simulated as ADC1 and ADC2 adsorption types (Figures 2, S4, and S5). For the case of acetaldehyde adsorbed onto the monomer surface model (denoted as  $\text{ADC}_{\text{Monomer}}^{\text{Acetaldehyde}}$ ), the intense absorption bands at 3722 and 3785  $\text{cm}^{-1}$  in the spectrum (Figure 2) were associated with the O–H stretching vibration. This suggests that the hydrogen bonds (H-bond) are formed between O

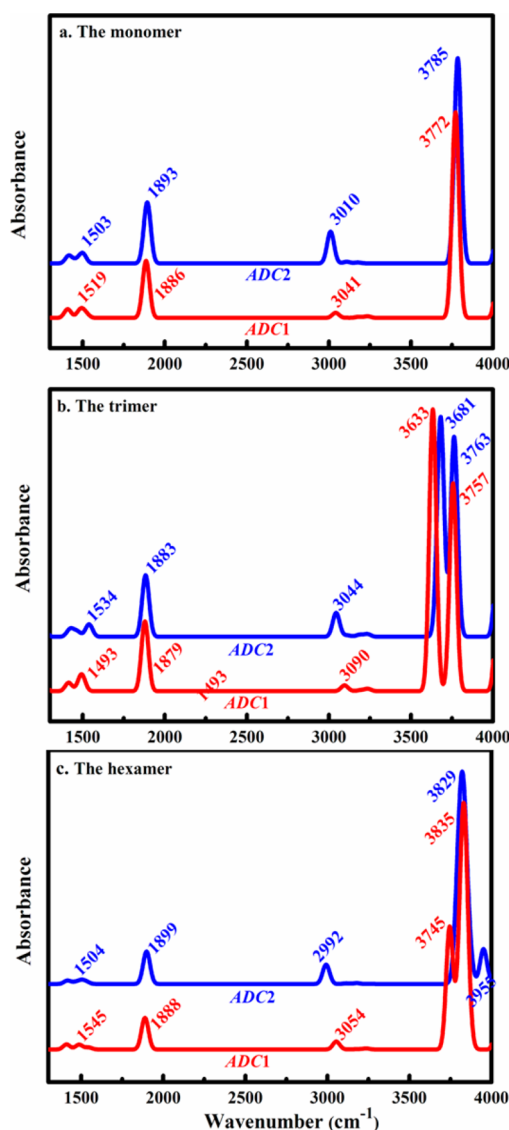


**Figure 2.** Calculated infrared spectrum for the complexes of acetaldehyde adsorbed onto three surface models. The infrared data are cut off at  $1300 \text{ cm}^{-1}$ , because of intense lattice absorptions.

atom of carbonyl group ( $\text{O}_{\text{Acetaldehyde}}$ ) and H atom of the silanol OH group ( $\text{H}_{\text{SiO}_2}$ ). As Figure 1 shows, the distances of H-bond ( $\text{O}_{\text{Acetaldehyde}} \cdots \text{H}_{\text{SiO}_2}$ ) in  $\text{ADC1}_{\text{Monomer}}^{\text{Acetaldehyde}}$  and  $\text{ADC2}_{\text{Monomer}}^{\text{Acetaldehyde}}$  are all approximately  $1.85 \text{ \AA}$ . Similar results were seen for propanal and butanal. For these, the H-bond formed between acetaldehyde and three surface models.

The frequencies of the infrared absorptions of acetaldehyde adsorbed onto the monomer surface model at 1519, 1886, and  $3041 \text{ cm}^{-1}$  for ADC1 adsorption type and at 1503, 1893, and  $3010 \text{ cm}^{-1}$  for ADC2 adsorption type, respectively, are very close to those in the gas phase. Characteristic peaks of the gas phase are 1461, 1919, and  $2968 \text{ cm}^{-1}$ .<sup>13</sup> Similar features apply to propanal and butanal. These results suggest that the studied aldehydes are weakly adsorbed onto the monomer surface model. For the three aldehydes adsorbed onto the trimer and hexamer surface models, the results aligned with the monomer surface model, except for the characteristic peaks of the trimer ( $3757$  and  $3763 \text{ cm}^{-1}$ ) and the hexamer surface models ( $3835$  and  $3829 \text{ cm}^{-1}$ ) (Figure 1).

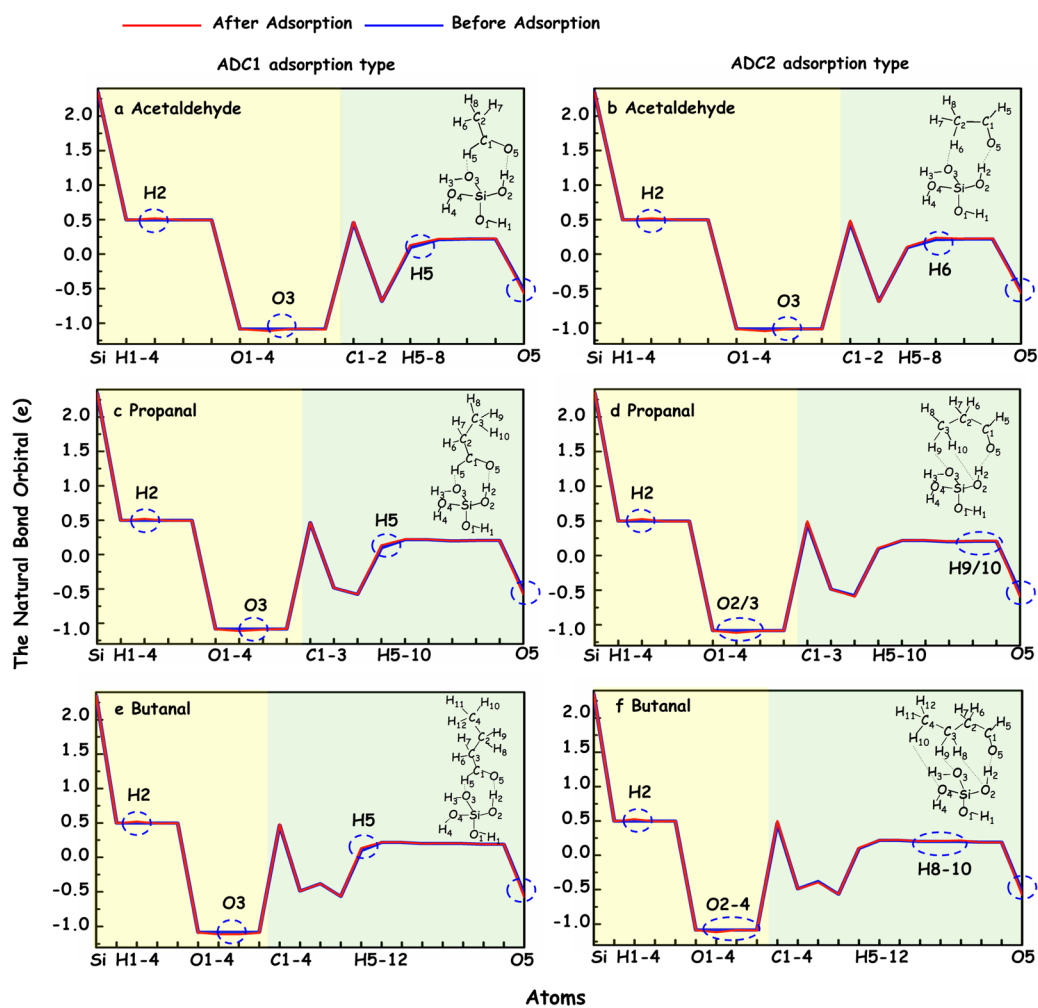


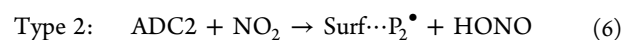
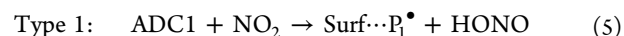
**Figure 3.** NBO charge distribution for the complexes of three aldehydes adsorbed onto the monomer surface model. The  $x$ -axis ordinate is atoms of adsorption complexes. The atoms that NBO charge changed mark with blue circles. The atoms of aldehydes and  $\text{SiO}_2$  are labeled as yellow and green backgrounds.

The natural bond orbital (NBO) charge distributions of adsorption complexes (ADC1 and ADC2) were also calculated to explore surface model adsorption properties. For the monomer surface model, Figure 3 shows that the NBO data of each atom changed little before and after the adsorption. For example, the NBO charges of the O atom in acetaldehyde are estimated to be  $-0.525$  and  $-0.569$  e, respectively, before and after it adsorbed onto the monomer surface model as an ADC1 adsorption type. Similar results were seen with the trimer and hexamer surface models. Thus, no change in the NBO charge further indicates that the interactions are not strong between the three studied aldehydes and the surface models.

Table S1 provides the adsorption energies ( $E_{\text{ae}}$ ) and shows that all  $E_{\text{ae}}$  values were negative, varying from  $-6.10$  to  $-8.72$  kcal mol $^{-1}$ . According to the group standard, the physical adsorption energy generally ranged from  $-1$  to approximately  $-10$  kcal mol $^{-1}$ , and the chemisorption processes generally had an energy of  $-10$  to approximately  $-191$  kcal mol $^{-1}$ .<sup>28</sup> Thus, the three studied aldehydes adsorbed onto the surface models all exhibit physical adsorption processes. However, all adsorption energies are negative, indicating that the adsorption processes are spontaneous in the atmosphere. Furthermore, as discussed in the Supporting Information, the  $E_{\text{ae}}$  displayed in Table S1 show that the outside H atoms that are free to be

attacked by  $\text{NO}_2$  are similar for three surface models, although there are some differences in the adsorption energies. Especially, increasing the model size of  $\text{SiO}_2$  requires significantly the computational time. As such, in this study, the monomer  $\text{Si}(\text{OH})_4$  was used as a good representative surface model to investigate heterogeneous reaction mechanisms and kinetics.

**Heterogeneous Reactions Mechanisms and Kinetics of Aldehydes Reacted with  $\text{NO}_2$ .** There are two kinds of adsorption complex types, yielding two corresponding reaction mechanisms, as follows:



where Surf stands for the surface;  $\text{P}^\bullet$  represents the corresponding H-abstraction product. Equations 5 and 6 were used as the basis for investigating reaction mechanisms and kinetics.

To confirm the above molecular structures correspond to a local minimum without an imaginary frequency, or to a saddle point with only one imaginary frequency, Table S2 lists the harmonic vibrational frequencies of the main stationary points, with available experimental data<sup>29</sup> for comparison. The results obtained at the MPWB1K/6-311G(d,p) level align with

available experimental data. The maximum relative errors are less than 8%, indicating the MPWB1K method is suitable for simulating the reaction model.

With respect to the Type 1 mechanism (Figures 4a, S6a, and S7a), due to aldehydes adsorbed onto the surface model

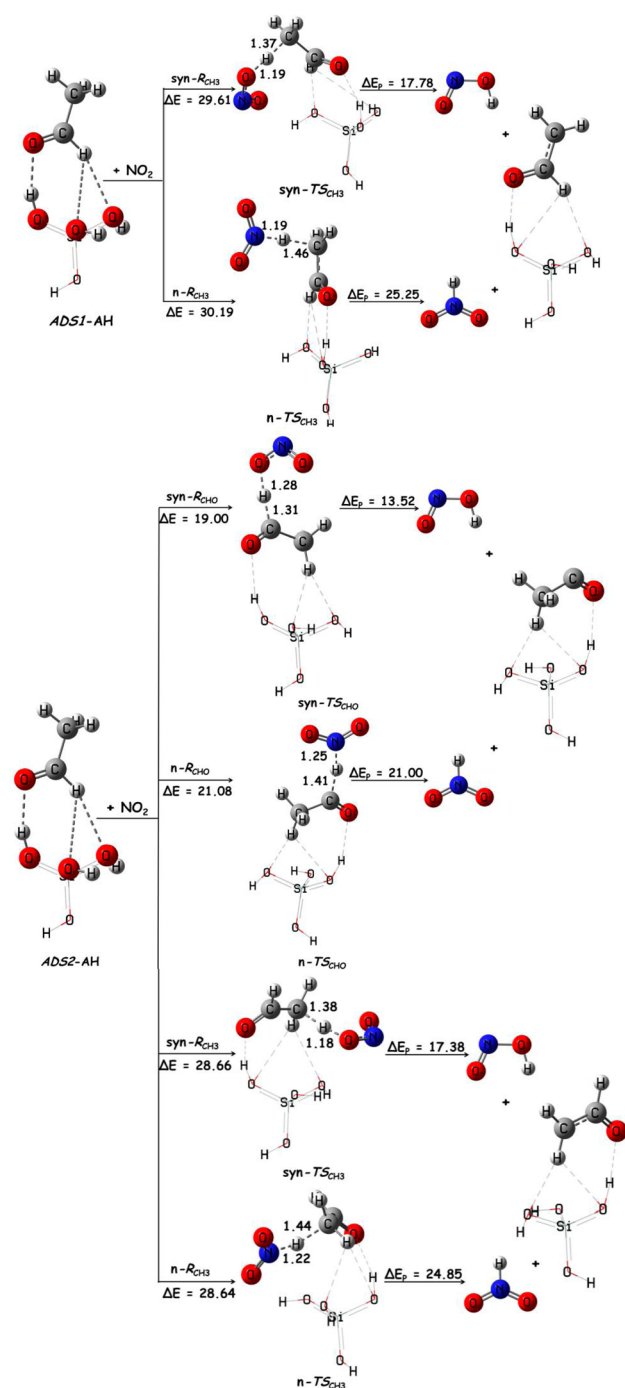


**Figure 4.** Schematic diagram of heterogeneous reactions of  $\text{NO}_2$  with acetaldehyde on the surface model embedded with the molecular structures (in Å) and the potential barriers (in  $\text{kcal mol}^{-1}$ ).

through the aldehydic H atom, only the H-abstraction channel of the alkyl group can be attacked by  $\text{NO}_2$  ( $\text{syn}/n\text{-R}_{\text{CH}_2/\text{CH}_3}$ ). Figures 4a, S6a, and S7a show the corresponding potential barriers ( $\Delta E$ ). For acetaldehyde, the  $\Delta E$  of  $\text{syn}$ -methyl-H-abstraction channel ( $\text{syn}-\text{R}_{\text{CH}_3}$ ) was  $28.89 \text{ kcal mol}^{-1}$ , slightly

lower than  $n$ -methene-H-abstraction channel ( $n\text{-R}_{\text{CH}_2}$ ). For propanal, the  $\Delta E$  of methene-H-abstraction ( $\text{syn}/n\text{-R}_{\text{CH}_2}$ ) channels were  $25.62$  and  $25.66 \text{ kcal mol}^{-1}$ , lower by 3–5  $\text{kcal mol}^{-1}$  than those of methyl-H-abstraction channels ( $\text{syn}/n\text{-R}_{\text{CH}_3}$ ). For butanal, the  $\Delta E$  of methene-H-abstraction channels ( $\text{syn}/n\text{-R}_{\text{CH}_2}$ ) were also lower than methyl-H-abstraction ( $\text{syn}/n\text{-R}_{\text{CH}_3}$ ) channels. These imply that for the Type 1 mechanism, the methene group ( $-\text{CH}_2$ ) in aldehydes is more readily attacked by  $\text{NO}_2$  than the methyl ( $-\text{CH}_3$ ) group.

For the Type 2 mechanism (Figures 4b, S6b, and S7b), both H atoms of the carbonyl group and alkyl group can be abstracted by  $\text{NO}_2$  ( $\text{syn}/n\text{-R}_{\text{CHO}}$  and  $\text{syn}/n\text{-R}_{\text{CH}_2/\text{CH}_3}$ ). As for acetaldehyde, the  $\Delta E$  of carbonyl-H-abstraction channels were  $19.00 \text{ kcal mol}^{-1}$  ( $\text{syn}-\text{R}_{\text{CHO}}$ ) and  $21.08 \text{ kcal mol}^{-1}$  ( $n\text{-R}_{\text{CHO}}$ ), at least  $7 \text{ kcal mol}^{-1}$  lower than those of methyl/methene-H-abstraction channels ( $\text{syn}/n\text{-R}_{\text{CH}_2/\text{CH}_3}$ ). This indicates that methyl/methene-H-abstraction channels may be negligible.

The  $\Delta E$  difference in the two carbonyl-H-abstraction channels ( $\text{syn}/n\text{-R}_{\text{CHO}}$ ) was  $2.08 \text{ kcal mol}^{-1}$ , implying that the  $\text{syn}-\text{R}_{\text{CHO}}$  channel is a major pathway, and the  $n\text{-R}_{\text{CHO}}$  channel is a minor pathway. Figures S6b and S7b show that other aldehydes (propanal and butanal) demonstrate similar behaviors. Moreover, for the studied aldehydes, the  $\Delta E$  of the  $\text{syn}-\text{R}_{\text{CHO}}$  channels in the Type 2 mechanism are at least  $6 \text{ kcal mol}^{-1}$  lower than those of methene-H-abstraction channels ( $\text{syn}/n\text{-R}_{\text{CH}_2}$ ) in the Type 1 mechanism. As discussed above, as the studied aldehydes are adsorbed onto the surface model, it is difficult for the Type 1 mechanism to take place. Instead, the Type 2 mechanism is favored to occur, by way of the CHO group abstracted by  $\text{NO}_2$ .

To further evaluate the channels' contributions and atmospheric impacts, each channel's rate constants and the total rate constants were investigated. To simulate the temperatures in all parts of the troposphere, the analysis considered the temperature range of  $217\text{--}298 \text{ K}$  (Tables S3–S5 and Figure S8). The branching ratios of  $\text{syn}-\text{R}_{\text{CHO}}$  channel for the three studied aldehydes all equaled 1. This indicates that the reactions of aldehydes with  $\text{NO}_2$  occurred almost exclusively by the carbonyl-H-abstraction channel ( $\text{syn}-\text{R}_{\text{CHO}}$ ) across the temperature range. All the other combined channels contribute less than 1% to the overall reaction. As Table S3 shows, the rate constant of the  $\text{syn}-\text{R}_{\text{CHO}}$  channel for the heterogeneous reaction of acetaldehyde with  $\text{NO}_2$  is  $8.00 \times 10^{-25} \text{ cm}^3 \text{ molecule}^{-1} \text{ s}^{-1}$ , which is 4–14 orders of magnitude faster than other channels. Similar conclusions can be drawn for propanal and butanal. Thus, the main products of the heterogeneous reactions of  $\text{NO}_2$  with three aldehydes were shown to be nitrous acid (HONO) and acyl radical across the investigated temperature range; the latter product (acyl radical) mainly remained on the  $\text{SiO}_2$  surface.

Figure S9 summarizes the total rate constants of the adsorbed aldehydes reactions with  $\text{NO}_2$ , calculations were  $8.00 \times 10^{-25}$ ,  $2.22 \times 10^{-24}$ , and  $2.80 \times 10^{-24} \text{ cm}^3 \text{ molecule}^{-1} \text{ s}^{-1}$  for acetaldehyde, propanal, and butanal, respectively, at  $298 \text{ K}$ . Values were  $3.78 \times 10^{-29}$ ,  $1.20 \times 10^{-28}$ , and  $1.32 \times 10^{-28} \text{ cm}^3 \text{ molecule}^{-1} \text{ s}^{-1}$  at  $217 \text{ K}$ . This means that the temperature increase benefits the heterogeneous reactions of the three aldehydes with  $\text{NO}_2$ . Furthermore, the relationship between the rate constants and the atmospheric temperatures were assessed to establish the Arrhenius formula. The corresponding formulas

were:  $2.03 \times 10^{-36} T^{7.77} \exp(-5932 \text{ K}/T) \text{ cm}^3 \text{ molecule}^{-1} \text{ s}^{-1}$  for acetaldehyde,  $4.31 \times 10^{-36} T^{7.61} \exp(-5951 \text{ K}/T) \text{ cm}^3 \text{ molecule}^{-1} \text{ s}^{-1}$  for propanal, and  $4.31 \times 10^{-34} T^{7.77} \exp(-6091 \text{ K}/T) \text{ cm}^3 \text{ molecule}^{-1} \text{ s}^{-1}$  for butanal (Table 1).

**Table 1. Modified Arrhenius Fit Parameters for  $k = AT^B \exp(-C/T)$  within the Temperature Range of 217–298 K**

reactions	$A^a$	$B$	$C^b$
acetaldehyde + NO <sub>2</sub>	$2.03 \times 10^{-36}$	7.77	5932
propanal + NO <sub>2</sub>	$4.31 \times 10^{-36}$	7.61	5951
butanal + NO <sub>2</sub>	$4.31 \times 10^{-33}$	7.15	6091

<sup>a</sup>Units in  $\text{cm}^3 \text{ molecule}^{-1} \text{ s}^{-1}$ . <sup>b</sup> $C = \frac{E}{R}$ ,  $E = E_a - nRT$ ,  $R$  is the gas constant.<sup>31</sup>

No experimental value was available for comparison, so the BMC–CCSD method was also used to assess the accuracy of dynamical model established using the MPWB1K//MPWB1K level. The  $n\text{-R}_{\text{CH}_3}$  channel in the Type 1 mechanism of the reaction of acetaldehyde with NO<sub>2</sub> was used as the sample reaction. The calculated energy parameters at the BMC–CCSD//MPWB1K/6-311G(d,p) were calculated to be 28.89 kcal mol<sup>-1</sup> for the potential barrier and 17.53 kcal mol<sup>-1</sup> for the reaction energy. This is in line with the corresponding values calculated at the MPWB1K//MPWB1K level (29.61 and 17.58 kcal mol<sup>-1</sup>). The calculated rate constants at two levels agree well in the measured temperature range 217–298 K, as shown in Figure S10. For example, the rate constants were  $2.65 \times 10^{-34} \text{ cm}^3 \text{ molecule}^{-1} \text{ s}^{-1}$  at the BMC–CCSD//MPWB1K level and  $1.79 \times 10^{-34} \text{ cm}^3 \text{ molecule}^{-1} \text{ s}^{-1}$  at the MPWB1K//MPWB1K level. These results further confirm that the established MPWB1K method in this study can effectively match an accurate and reliable reaction model.

To further evaluate specific rate constants at different atmospheric heights, the relationship between the rate constants and different altitudes were analyzed; they are presented in Tables S3–S5. In general, the tropospheric temperature drops approximately 6.49 K for every 1 km in altitude, whereas the stratosphere temperature is kept constant at 216.69 K (from 11 km height above the earth surface).<sup>30</sup> Table S3 shows that the rate constants decrease from  $8.00 \times 10^{-25}$  to  $3.78 \times 10^{-29} \text{ cm}^3 \text{ molecule}^{-1} \text{ s}^{-1}$  as the altitude increases from 0 to 12 km. This suggests that for the heterogeneous reaction of adsorbed acetaldehyde with NO<sub>2</sub> onto the SiO<sub>2</sub> surface, rate constants will become slower as the altitude rises. Similar results were seen for propanal and butanal (Tables S4 and S5). It is worth noting, however, that VOC and mineral particle concentrations significantly decrease as the altitude increases. As such, the reaction impacts at higher altitudes require further confirmation with experimental data.

**Table 2. Adsorption Energies ( $\Delta E_{\text{ae}}$ ), Potential Barriers ( $\Delta E$ , kcal mol<sup>-1</sup>), and the Rate Constants ( $k$ , cm<sup>3</sup> molecule<sup>-1</sup> s<sup>-1</sup>) for the Heterogeneous and Homogeneous Reactions of NO<sub>2</sub> with Acetaldehyde, Propanal, and Butanal**

	$\Delta E_{\text{ae}}^a$	$\Delta E$		$k^b$	
		hetero	<sup>e</sup> homo	hetero	<sup>d</sup> homo
acetaldehyde	-6.10	19.00	18.79	$8.00 \times 10^{-25}$	$1.44 \times 10^{-24}$
propanal	-6.48	18.42	18.11	$2.22 \times 10^{-24}$	$3.43 \times 10^{-24}$
butanal	-6.94	18.66	17.48	$2.80 \times 10^{-24}$	$1.85 \times 10^{-23}$

<sup>a</sup>The values of the most stable adsorption configurations (in kcal mol<sup>-1</sup>); <sup>b</sup>The data from reference.<sup>13</sup>

To systemically understand the effect of SiO<sub>2</sub> on the reactions of the three studied aldehydes with NO<sub>2</sub>, Table 2 lists the parameters assessed, including the adsorption energy, the potential barriers, and the rate constants, both in the absence<sup>13</sup> and in the presence of SiO<sub>2</sub>. For acetaldehyde, the  $\Delta E$  in the presence of SiO<sub>2</sub> is 19.00 kcal mol<sup>-1</sup>, higher by 0.21 kcal mol<sup>-1</sup> than the reaction without SiO<sub>2</sub>. The calculated rate constants are approximately half of the corresponding values of the homogeneous reaction. This means that the presence of SiO<sub>2</sub> will enhance the potential barriers of the reaction of acetaldehyde with NO<sub>2</sub> and depress the reaction rate. Similar results were seen with the other two aldehydes. In other words, silica can slow the rate constants of the reactions of the three studied aldehydes with NO<sub>2</sub>, and reduce the probability of air pollution from these atmospheric reactions. This study established the theoretical model upon which to further investigate this effect on VOC atmospheric reactions.

## CONCLUSION

This work successfully established a computational approach to assess the adsorption performances of C2–C4 aliphatic aldehydes and NO<sub>2</sub> onto the surface of SiO<sub>2</sub>. It also established their heterogeneous reaction mechanisms and kinetics. Key findings were as follows:

- Theoretical results closely agree with published data and other comparable calculation methods, validating that the current computational approach is a reasonable and cost-effective method to reveal the adsorption mechanism of C2–C4 aliphatic aldehydes and NO<sub>2</sub>, as well as their heterogeneous reaction mechanisms.
- The results of the spectral features and the adsorption parameter analyses show that hydrogen bonds can be formed between aliphatic aldehydes with SiO<sub>2</sub> with negative adsorption energies. These data provide evidence for the adsorption processes, which can happen spontaneously. The adsorption mechanisms suggest that SiO<sub>2</sub> is a sink for atmospheric aliphatic aldehydes.
- When the reaction mechanisms and kinetics of adsorbed aldehydes with NO<sub>2</sub> are investigated, results show that the H-abstraction from the CHO group of aldehydes by NO<sub>2</sub> is an exclusive pathway, forming nitrous acid and acyl radicals. Increasing temperatures benefit the heterogeneous reactions of NO<sub>2</sub> with three aldehydes. The order of rate constant is obtained as  $k(\text{acetaldehyde}) < k(\text{propanal}) < k(\text{butanal})$ .
- SiO<sub>2</sub> enhances the intrinsic reaction barrier and depresses the rate constants of NO<sub>2</sub> reactions with C2–C4 aliphatic aldehydes. This means that silica can slow the reaction of three studied aldehydes with NO<sub>2</sub>, reducing the probability of air pollution.

**■ ASSOCIATED CONTENT****■ Supporting Information**

The Supporting Information is available free of charge on the ACS Publications website at DOI: 10.1021/acs.jpca.5b09065.

Method of rate constant calculation. Description of adsorption of aldehydes onto the surface. Tables of adsorption energies, frequencies, and kinetics data in the absence and presence of SiO<sub>2</sub>. Structural geometries, IR spectra, diagram of heterogeneous reactions, plot of calculated branching ratio and rate constants versus 1000/T, and Cartesian coordinates. (PDF)

**■ AUTHOR INFORMATION****Corresponding Author**

\*Taicheng An. Tel: 86-20-85291501. Fax: 86-20-85290706. E-mail address: antc99@gig.ac.cn.

**Notes**

The authors declare no competing financial interest.

**■ ACKNOWLEDGMENTS**

This is contribution No. IS-2146 from GIGCAS. This work was financially supported by National Natural Science Foundation of China (41205088 and 41373102), National Natural Science Funds for Distinguished Young Scholars (41425015), the Team Project from Natural Science Foundation of Guangdong Province, China (S2012030006604), and Special Fund of SKLOG2013A01. We also want to thank Professor Donald G. Truhlar for his providing POLYRATE program.

**■ REFERENCES**

- (1) Bian, H. S.; Zender, C. S., Mineral Dust and Global Tropospheric Chemistry: Relative Roles of Photolysis And Heterogeneous Uptake. *J. Geophys. Res.* **2003**, *108*, DOI 10.1029/2002JD003143.
- (2) Davesne, E.; Dideriksen, K.; Christiansen, B. C.; Sonne, M.; Ayala-Luis, K. B.; Koch, C. B.; Hansen, H. C. B.; Stipp, S. L. S. Free Energy of Formation for Green Rust Sodium Sulphate ((NaFe6-Fe3III)-Fe-II(OH)(18) (SO4)(2(s))). *Geochim. Cosmochim. Acta* **2010**, *74*, 6451–6467.
- (3) Shen, X. L.; Zhao, Y.; Chen, Z. M.; Huang, D. Heterogeneous Reactions of Volatile Organic Compounds in the Atmosphere. *Atmos. Environ.* **2013**, *68*, 297–314.
- (4) Choobari, O. A.; Zavar-Reza, P.; Sturman, A. The Global Distribution of Mineral Dust and Its Impacts on the Climate System: A Review. *Atmos. Res.* **2014**, *138*, 152–165.
- (5) Galy-Lacaux, C.; Carmichael, G. R.; Song, C. H.; Lacaux, J. P.; Al Ourabi, H.; Modi, A. I. Heterogeneous Processes Involving Nitrogenous Compounds and Saharan Dust Inferred from Measurements and Model Calculations. *J. Geophys. Res.* **2001**, *106*, 12559–12578.
- (6) Iuga, C.; Olea, R. E.; Vivier-Bunge, A. Mechanism and Kinetics of the OH· Radical Reaction with Formaldehyde Bound to an Si(OH)<sub>4</sub> Monomer. *J. Mex. Chem. Soc.* **2008**, *52*, 36–46.
- (7) Zhao, Y.; Chen, Z. M.; Zhao, J. N. Heterogeneous Reactions of Methacrolein and Methyl Vinyl Ketone on alpha-Al<sub>2</sub>O<sub>3</sub> Particle. *Environ. Sci. Technol.* **2010**, *44*, 2035–2041.
- (8) Tong, S. R.; Wu, L. Y.; Ge, M. F.; Wang, W. G.; Pu, Z. F. Heterogeneous Chemistry of Monocarboxylic Acids on Alpha-Al<sub>2</sub>O<sub>3</sub> at Different Relative Humidities. *Atmos. Chem. Phys.* **2010**, *10*, 7561–7574.
- (9) Iuga, C.; Sainz-Diaz, C. I.; Vivier-Bunge, A. On the OH Initiated Oxidation of C2-C5 Aliphatic Aldehydes in the Presence of Mineral Aerosols. *Geochim. Cosmochim. Acta* **2010**, *74*, 3587–3597.
- (10) Clarisse, B.; Laurent, A. M.; Seta, N.; Le Moullec, Y.; El Hasnaoui, A.; Momas, I. Indoor Aldehydes: Measurement of Contamination Levels and Identification of Their Determinants in Paris Dwellings. *Environ. Res.* **2003**, *92*, 245–253.

(11) Roda, C.; Barral, S.; Ravelomanantsoa, H.; Dusseaux, M.; Tribout, M.; Le Moullec, Y.; Momas, I. Assessment of Indoor Environment in Paris Child Day Care Centers. *Environ. Res.* **2011**, *111*, 1010–1017.

(12) Atkinson, R. Atmospheric Chemistry of VOCs and NO<sub>x</sub>. *Atmos. Environ.* **2000**, *34*, 2063–2101.

(13) Ji, Y. M.; Gao, Y. P.; Li, G. Y.; An, T. C. Theoretical Study of the Reaction Mechanism and Kinetics of Low-Molecular-Weight Atmospheric Aldehydes (C1-C4) with NO<sub>2</sub>. *Atmos. Environ.* **2012**, *54*, 288–295.

(14) Zhou, X. L.; Mopper, K. Measurement of Sub-Parts-Per-Billion Levels of Carbonyl-Compounds in Marine Air by a Simple Cartridge Trapping Procedure Followed by Liquid-Chromatography. *Environ. Sci. Technol.* **1990**, *24*, 1482–1485.

(15) Iuga, C.; Vivier-Bunge, A.; Hernandez-Laguna, A.; Sainz-Diaz, C. I. Quantum Chemistry and Computational Kinetics of the Reaction between OH Radicals and Formaldehyde Adsorbed on Small Silica Aerosol Models. *J. Phys. Chem. C* **2008**, *112*, 4590–4600.

(16) Gomes, L.; Gillette, D. A. A Comparison of Characteristics of Aerosol from Dust Storms in Central-Asia with Soil-Derived Dust from Other Regions. *Atmos. Environ., Part A* **1993**, *27*, 2539–2544.

(17) Frisch, M. J.; et al. GAUSSIAN 03, Revision A.1; Gaussian, Inc.: Pittsburgh, PA, 2003.

(18) Ji, Y. M.; Wang, H. H.; Li, G. Y.; An, T. C. Theoretical Investigation on the Role of Mineral Dust Aerosol in Atmospheric Reaction: A Case of the Heterogeneous Reaction of Formaldehyde with NO<sub>2</sub> onto SiO<sub>2</sub> Dust Surface. *Atmos. Environ.* **2015**, *103*, 207–214.

(19) Zhao, Y.; Truhlar, D. G. Hybrid Meta Density Functional Theory Methods for Thermochemistry, Thermochemical Kinetics, and Noncovalent Interactions: The MPW1B95 and MPWB1K Models and Comparative Assessments for Hydrogen Bonding and van der Waals Interactions. *J. Phys. Chem. A* **2004**, *108*, 6908–6918.

(20) Lynch, B. J.; Zhao, Y.; Truhlar, D. G. The 6-31B(d) Basis Set and the BMC-QCISD and BMC-CCSD Multicoefficient Correlation Methods. *J. Phys. Chem. A* **2005**, *109*, 1643–1649.

(21) Zhao, Y.; Schultz, N. E.; Truhlar, D. G. Design of Density Functionals by Combining the Method of Constraint Satisfaction with Parametrization for Thermochemistry, Thermochemical Kinetics, and Noncovalent Interactions. *J. Chem. Theory Comput.* **2006**, *2*, 364–382.

(22) Chuang, Y. Y.; Corchado, J. C.; Truhlar, D. G. Mapped Interpolation Scheme for Single-Point Energy Corrections in Reaction Rate Calculations and a Critical Evaluation of Dual-Level Reaction Path Dynamics Methods. *J. Phys. Chem. A* **1999**, *103*, 1140–1149.

(23) Norton, K. P.; von Blanckenburg, F. Silicate Weathering of Soil-Mantled Slopes in an Active Alpine Landscape. *Geochim. Cosmochim. Acta* **2010**, *74*, 5243–5258.

(24) Liu, Y. P.; Lu, D. H.; Gonzalezfont, A.; Truhlar, D. G.; Garrett, B. C. Direct Dynamics Calculation of the Kinetic Isotope Effect for an Organic Hydrogen-Transfer Reaction, Including Corner-Cutting Tunneling in 21 Dimensions. *J. Am. Chem. Soc.* **1993**, *115*, 7806–7817.

(25) Pereira, J. C. G.; Catlow, C. R. A.; Price, G. D. Ab Initio Studies of Silica-Based Clusters. Part II. Structures and Energies of Complex Clusters. *J. Phys. Chem. A* **1999**, *103*, 3268–3284.

(26) Pereira, J. C. G.; Catlow, C. R. A.; Price, G. D. Ab Initio Studies of Silica-Based Clusters. Part I. Energies and Conformations of Simple Clusters. *J. Phys. Chem. A* **1999**, *103*, 3252–3267.

(27) Moravetski, V.; Hill, J. R.; Eichler, U.; Cheetham, A. K.; Sauer, J. Si-29 NMR Chemical Shifts of Silicate Species: Ab Initio Study of Environment and Structure Effects. *J. Am. Chem. Soc.* **1996**, *118*, 13015–13020.

(28) Nollet, H.; Roels, M.; Lutgen, P.; Van der Meeren, P.; Verstraete, W. Removal of PCBs from Wastewater using Fly Ash. *Chemosphere* **2003**, *53*, 655–665.

(29) NIST, available at <http://webbook.nist.gov/chemistry/>, last access March 2015.

(30) Ji, Y. M.; Wang, H. H.; Gao, Y. P.; Li, G. Y.; An, T. C. A Theoretical Model on the Formation Mechanism and Kinetics of Highly Toxic Air Pollutants from Halogenated Formaldehydes

Reacted with Halogen Atoms. *Atmos. Chem. Phys.* **2013**, *13*, 11277–11286.

(31) Zheng, J. J.; Truhlar, D. G. Kinetics of Hydrogen-Transfer Isomerizations of Butoxyl Radicals. *Phys. Chem. Chem. Phys.* **2010**, *12*, 7782–7793.